Optimizing Group Transfer Catalysis by Copper Complex with Redox-Active Ligand in an Entatic State

Yufeng Ren, Jeremy Forte, Khaled Cheaib, Nicolas Vanthuyne, Louis Fensterbank, Hervé Vezin, Maylis Orio, Sébastien Blanchard, Marine Desage-El Murr

Optimizing Group Transfer Catalysis by Copper Complex with Redox-active Ligand in an Entatic State

Y. Ren, J. Forté, K. Cheaib, N. Vanthuyne, L. Fensterbank, H. Vezin, M. Orio, S. Blanchard, M. Desage-El Murr

PII: S2589-0042(20)30139-5

DOI: https://doi.org/10.1016/j.isci.2020.100955

Reference: ISCI 100955

To appear in: *ISCIENCE*

Received Date: 24 September 2019

Revised Date: 14 January 2020

Accepted Date: 25 February 2020

Please cite this article as: Ren, Y., Forté, J., Cheaib, K., Vanthuyne, N., Fensterbank, L., Vezin, H., Orio, M., Blanchard, S., Desage-El Murr, M., Optimizing Group Transfer Catalysis by Copper Complex with Redox-active Ligand in an Entatic State, *ISCIENCE* (2020), doi: https://doi.org/10.1016/j.isci.2020.100955.

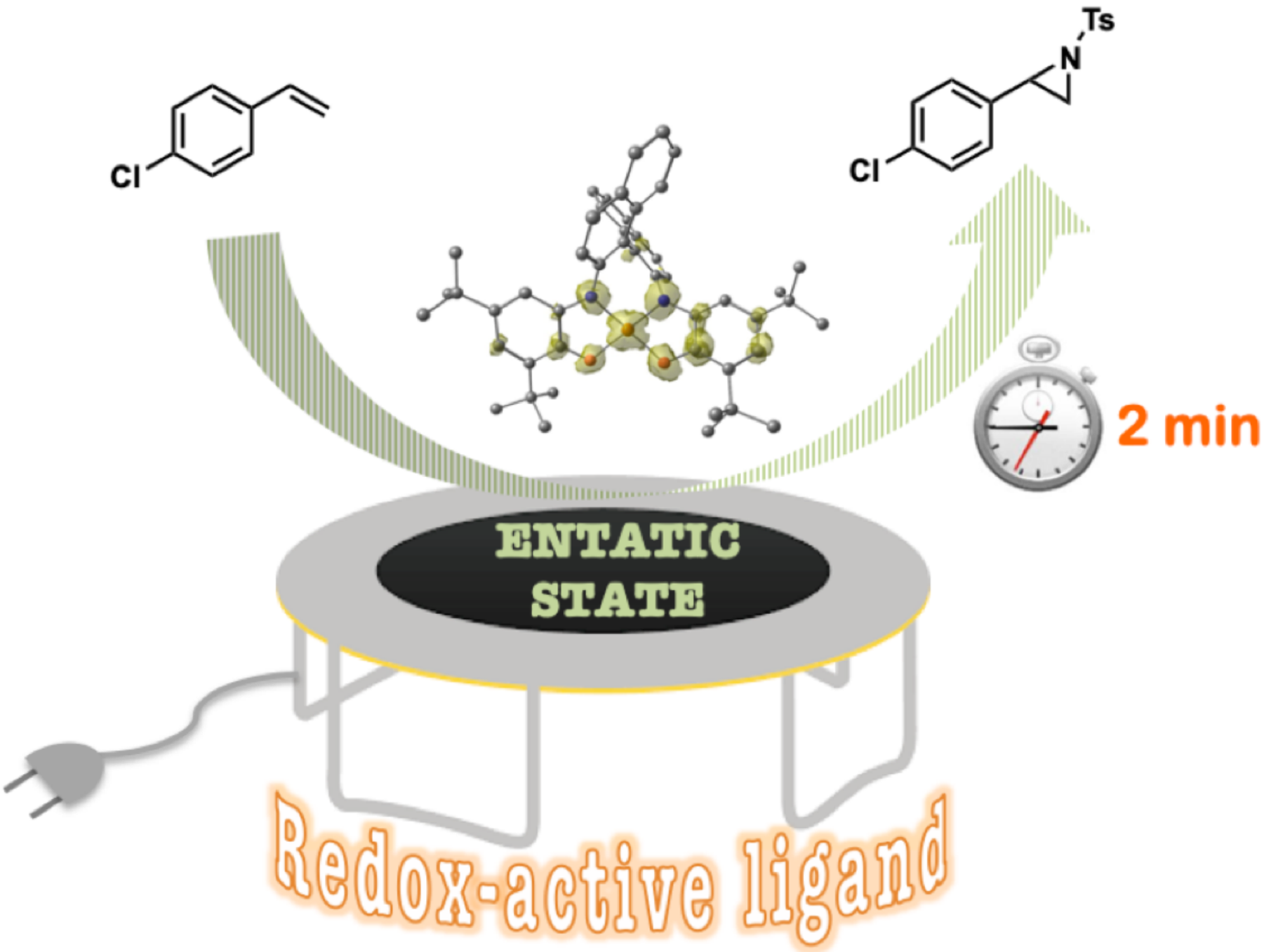
Cl
Ts
N
Cl
2 min
ENTATIC
STATE
Redox-active ligand

Optimizing Group Transfer Catalysis by Copper Complex with Redox-active Ligand in an Entatic State

Y. Ren,[1] J. Forté,[1] K. Cheaib,[1] N. Vanthuyne,[2] L. Fensterbank,[1] H. Vezin,[3] M. Orio,[2] S. Blanchard,[1] and M. Desage-El Murr[4,5,*]

[1]Sorbonne Université, Institut Parisien de Chimie Moléculaire, UMR CNRS 8232, 75005 Paris, France
[2]Aix Marseille Université, CNRS, Centrale Marseille, iSm2, UMR CNRS 7313, 13397 Marseille, France
[3]Université des Sciences et Technologies de Lille, LASIR, UMR CNRS 8516, 59655 Villeneuve d'Ascq Cedex, France
[4] Université de Strasbourg, Institut de Chimie, UMR CNRS 7177, 67000 Strasbourg, France
[5]Lead Contact
*Correspondence: desageelmurr@unistra.fr

SUMMARY

Metalloenzymes use earth-abundant non-noble metals to perform high-fidelity transformations in the biological world. To ensure chemical efficiency, metalloenzymes have acquired evolutionary reactivity-enhancing tools. Among these, the entatic state model states that a strongly distorted geometry induced by ligands around a metal center gives rise to an energized structure called entatic state, strongly improving the reactivity. However, while the original definition refers both to the transfer of electrons or chemical groups, the chemical application of this concept in synthetic systems has mostly focused on electron transfer, therefore eluding chemical transformations. Here we report that a highly-strained redox-active ligand enables a copper complex to perform catalytic nitrogen- and carbon-group transfer in as fast as two minutes, thus exhibiting a strong increase in reactivity compared to its unstrained analogue. This report combines two reactivity-enhancing features from metalloenzymes, entasis and redox cofactors, applied to group-transfer catalysis.

bioinspired catalysis • metalloenzyme mimics • redox-active ligand • entatic state • earth-abundant metals

INTRODUCTION

The biological world offers potential clues to solve the current pressing energy and resources-related issues (Adesina *et al.*, 2017; Rudroff *et al.*, 2018). The efficiency of biological catalytic systems faces chemists with the challenges of transferring enzymatic performance into synthetic small-molecule catalysts using non noble metals. Metalloenzymes use earth-abundant *3d* metals and amino acid-derived coordination spheres to achieve complex (multi)electronic transformations required for small-molecule activation and atom transfer reactions. To fulfil these stringent criteria of natural resources, metalloenzymes have evolved reactivity-enhancing strategies aimed at performing such difficult transformations through more favourable thermodynamic pathways. The entatic state concept stems from the observation that single molecule coordination complexes designed as metalloenzymes models often fail to exhibit properties similar to the natural metalloenzymatic active sites (Vallee and Williams, 1968; Williams, 1971; Williams, 1995; Stanek, Hoffmann and Herres-Pawlis, 2018). It was thus suggested that secondary and tertiary structures induced by amino acid-based side chains in proteins provide distortions in the coordinative environment that endow the metal center with enhanced reactivity, to which Vallée and Williams refer as "a catalytically poised state" (Vallee and Williams, 1968). Strikingly, a strong link between local geometric frustration induced by tertiary structure effects around enzymatic catalytic sites and their catalytic activity has recently been unveiled (Freiberger *et al.*, 2019). Frustration patterns were demonstrated to be evolutionary highly conserved, more than the primary structure or residues forming the

catalytic site itself, which establishes the central relevance of coordinative distortion to enzymatic catalytic activity.

Entasis is well-known in copper proteins involved in electron transfer such as blue copper proteins and has traditionally been studied in the context of Cu^{I}/Cu^{II} oxidation states. When tetracoordinated, these two oxidation states have distinct geometric requirements from tetrahedral to square planar, and the entatic state exhibits an in-between distorted geometry that minimizes energetic penalties arising from coordinative reorganization (Fig. 1a). Possible designs for coordination spheres inducing ligand misfit have been discussed by Comba (Comba, 2000). The majority of reports involve two ditopic or one cyclic tetradentate ligands and include systems with biphenyl subunits (Malachowski, 1999; Müller, 1996, Müller, 1988), multiple bonds and rigid or substituted structures, carbohydrate backbones (Garcia *et al.*, 2015) and guanidinoquinoline ligands (Hoffmann Alexander *et al.*, 2013; Stanek Julia *et al.*, 2017). More recently, the entatic state concept was extended to photoinduced electronic transfers (Dicke 2018) thus showing the continued relevance of this biomimetic feature in electron transfer chemistry. While most studies focus on electron transfer involving a Cu^{I}/Cu^{II} redox couple, the seminal article by Vallée and Williams (Vallee and Williams, 1968) states that entatic behavior arising from ligand misfit also extends to enzymatic metallic sites performing "transfer of an atom, radical, or a group", as well as higher metallic oxidation states such as Co^{II}/Co^{III} in corrin enzymes and Fe^{II}/Fe^{III} (Mara, 2017). A recent report on the hydroxylation of methane to methanol by heterogeneous catalysis performed by iron-containing zeolithes demonstrates that the zeolithe lattice induces a matrix strain which activates a square planar Fe(II) site into a Fe(IV)=O reactive center through entasis (Snyder *et al.*, 2016), and a bispidine Fe(IV)=O species in an entatic state has been reported to perform oxygen-group transfer in homogeneous catalysis (Comba *et al.*, 2016). These examples of oxygen-group transfer systems, which emulate natural systems' catalytic arsenal, provide great opportunities for the design of synthetic systems able to perform highly-desired transformations such as multi-electronic small-molecule activation. However, to date, no synthetic catalytic system was demonstrated to perform group-transfer other than oxygen through the entatic state model.

Just as the entatic state principle provides a fruitful trail of inspiration for coordination chemists, other biomimetic strategies, related to electron transfer, focus on enzymatic redox co-factors that provide electrons to the active sites (Stubbe and van der Donk, 1998; Davidson, 2018). Such systems are known as redox-active ligands. This field of research is morphing into an area of intense development aimed at harnessing the potential of systems with rich redox flexibility (Grützmacher, 2008; Chirik and Wieghardt, 2010; Praneeth, Ringenberg and Ward, 2012; van der Vlugt, 2012; Blanchard *et al.*, 2012; Lyaskovskyy and de Bruin, 2012; Luca and Crabtree, 2012; Broere, Plessius and Vlugt, 2015; van der Vlugt, 2019; Albold *et al.*, 2019). Recently, an entatic pair of copper complexes bearing redox-active guanidine ligands was shown to enable fine-tuning between metal- and ligand-based electronic transfers (Schrempp *et al.*, 2017). This structural study was the first report interfacing the two concepts of entasis and redox-active ligands, and was focused on the electronic behavior of the entatic pair. Using redox-active copper complex $Cu(SQ)_2$ (SQ : iminosemiquinone) originally developed as a Galactose Oxidase (GAO) model (Chaudhuri et al., 1998; Chaudhuri et al., 2001), we have shown that ligand-based redox activity influences the overall reactivity of the complex towards electron transfer (Jacquet, Blanchard, *et al.*, 2016; Jacquet *et al.*, 2017), C–N bond formation (Jacquet, Chaumont, *et al.*, 2016) and nitrogen group transfer (Ren *et al.*, 2018) while preserving a Cu(II) oxidation state. Here we report an acyclic tetradentate redox-active ligand exhibiting C_2 symmetry with overall three possible rotations around single bonds (degrees of freedom). This particular geometry induces enhanced catalytic reactivity of resulting complex **1** through entasis. This specific ligand design combines an atropisomeric backbone, which enforces chirality and exerts an outward strain, with a redox-active iminosemiquinone/iminobenzoquinone ONNO coordination sphere which pulls in the opposite inward direction towards metal chelation (Fig. 1b). These conflicting steric demands induce a coordination stress while the bridging binaphtalene backbone installs full conjugation between the two redox-active units, resulting in enhanced electronic delocalization. Complex **1** performs catalytic nitrogen and carbon group transfer in as fast as two minutes on a model substrate, and exhibits up to a forty-fold increase in synthetic efficiency compared to its unstrained analogue $Cu(SQ)_2$. Moreover, it can convert sterically

hindered or unactivated alkenes. The present work shows that interfacing two reactivity-enhancing features from metalloenzymes, such as entasis and redox cofactors, can improve group-transfer catalysis.

RESULTS

Complex synthesis and structural studies

Condensation of two *tert*-butylcatechol with 1,1'-binaphthyl-2,2'-diamine yields easy access to 1,1'-binaphtyl-2,2'-diaminophenol (hereafter noted BINap) ligand (Figure 2a and SI), and its structure was confirmed by X-ray crystallography (Fig. 1c). Aerobic complexation of BINap ligand **2** with copper chloride affords complex Cu(BINap-SQ_2) **3** as a green solid. The spectroscopic signature of **3** is very similar to those of $Cu(SQ)_2$ **4** (Fig. 2b) and $Cu(L_{Biphen}SQ_2)$, a copper complex reported by Chaudhuri and incorporating a biphenyl unit instead of the atropisomeric binaphthyl unit (Mukherjee *et al.*, 2008). At 10 K, **3** displays a S=1/2 signal centered on the copper (Fig. S10), as attested by the strong anisotropy of the EPR spectrum and the presence of hyperfine coupling with the I=3/2 copper nucleus. The doublet ground spin state of **3** is further supported by DFT calculations (Supplementary Table S15). The UV-vis spectrum of **3** (Fig. 2d) presents the expected ligand to ligand (SQ to SQ) charge transfer band around 900 nm (800 nm in **4** and 880 nm in $Cu(L_{Biphen}SQ_2)$) which points towards **3** as a Cu(II) complex bearing a dianionic diradical $BINapSQ_2$ ligand. This description is in agreement with the DFT-calculated electronic structure of **3** (Fig. S110-111). The cyclic voltammogram of **3** displays four reversible waves (two oxidative and two reductive, Supplementary Fig. S9) at redox potentials very close to those of the parent complexes, indicating similar electronic structures and ligand-based redox processes (Supplementary Tables S1-2).

Oxidation of Cu(BINap-SQ_2) **3** with Br_2 followed by halide abstraction led to the formation of fully oxidized $[Cu(BINap\text{-}BQ_2)]^{2+}$ **5**. The singly oxidized complex $[Cu(BINap\text{-}SQ\text{-}BQ)]^{+}$ **1** can be prepared either by oxidation of **3** with 1 equiv. $AgPF_6$ or by mediamutation between an equimolar mixture of complexes **3** and **5** (see SI). Cyclic voltammograms of **1** and **5** are very similar to that of **3** and only differ by the onset potential, thus attesting the chemical reversibility of the redox processes. While **1** is X-band EPR silent at 10 K, **5** displays an EPR spectrum in agreement with an S=1/2 ground state centered on the copper (Fig. S13). The doublet ground spin state of **5** has been also predicted by DFT calculations (Fig. S113-114). The UV-vis spectrum of **1** displays around 1200 nm a LLCT band associated with the oxidation of a SQ moiety into BQ, whereas no LLCT can be identified for fully oxidized **5** (Fig. 2d). This is reminiscent of the parent complexes and confirms that the two oxidation processes are ligand-centered. Enantiopure R or S complexes of **1** and **3** can be synthesized from enantiopure R or S forms of **2**, as attested by circular dichroism and chiral HPLC analysis (Fig. S3,S5).

Figure 1. Design of a redox-active ligand creating a vacant coordination site at metal through strong coordination distortion.
a, The entatic state reactivity model for electron and group transfer in a tetracoordinated copper complex. b, Structure of complex **1** $[CuBINap\ (SQ\text{-}BQ)]^{+}$. c, X-ray crystal structure of ligand **2** representing the associated strains. d, X-ray crystal structure of complex **1** exhibiting a pentacoordinated coordination sphere resulting from coordination strain.

Figure 2. Synthesis and spectroscopic studies for complex 1.
a, Synthetic scheme for complex **1**, reaction conditions: a) CuCl (1 equiv.), Et_3N (4 equiv.), dry acetonitrile; b) AgOTf (1 equiv.). b, Unstrained complex $Cu(SQ)_2$ **4**. c, Cyclic voltammogram of complex **1**. d, UV-vis-NIR spectrum of $[Cu(BINap\text{-}SQ\text{-}BQ)]^{+}$ **1** (purple), Cu(BINap-SQ_2) **3** (green) and $[Cu(BINap\text{-}BQ_2)]^{2+}$ **5** (see SI for structure, red); 0.1 mM in DCM at rt. e, Circular dichroism spectrum of racemate and enantiopure $[Cu(BINap\text{-}SQ\text{-}BQ)]^{+}$ **1** (C=0.3 mM).

Attempts to grow crystals of **3** led to very weakly diffracting samples, with maximum resolution of 1.29 Å (see SI) which indicate that the copper centre is in coordinence 4 (N_2O_2 of BINap). Crystals suitable for X-ray diffraction were obtained on racemate and enantiopure samples of complex **1** and revealed that the coordination sphere is completed by an aquo ligand to provide a square pyramidal environment in which an oxygen atom of the BINap occupies the axial position, and not the water molecule (From a CCDC database search, out of 126 structures of 5-coordinated Cu complexes bearing $\{(NCCO)_2 + OH_2\}$

coordination sphere, only five do not display a square pyramidal geometry with water as apical ligand) (Fig. 1d). This unusual coordination sphere can be explained by the coordination stress resulting from the design of ligand **2**, and the singly oxidized SQ-BQ redox-active subunit, which bears increased electrophilicity compared to complex **3**. The combination of these unique steric and electronic features induces a distorted pentacoordinated sphere with a newly occupied coordination site. The atropisomeric backbone exerts an outward strain associated to the large torsion angle between the two naphthalene rings (99.9° in free ligand **2**, 66.7° in the complex), and opposes to N_2O_2 and Cu being in the same plane. The long axial Cu-O_{BINap} distance (2.309(2)Å) indicates a weak coordination. Detailed analysis of the bond distances in coordinated BINap ligand shows that this O atom belongs to the benzoquinone part of the ligand (bond lengths in this part of the ligand of $d_{C\text{-}O}$ = 1.235(4)Å, $d_{C\text{-}C}$ = 1.519(15)Å and $d_{C\text{-}N}$ = 1.289(5)Å) while the in plane half of the ligand corresponds to the iminosemiquinone moiety ($d_{C\text{-}O}$ = 1.288(4)Å, $d_{C\text{-}C}$ = 1.455(5)Å and $d_{C\text{-}N}$ = 1.344(4)Å) (Chaudhuri *et al.*, 2001). Such deviation from square planar geometry has been reported in the context of a salen-based Cu^{II} GAO functional mimic with an atropisomeric backbone by Stack and co-workers (Wang *et al.*, 1998). DFT calculations provided insights into the electronic features of complex **1** which can be assigned as a Cu(II) center bound to a radical BINap ligand (Fig. S113,114). The system is characterized by a triplet S=1 ground spin state due to moderate ferromagnetic coupling between the metal center and the ligand radical moiety (Supplementary Table S15). A singlet S=0 state is close enough in energy to be thermally populated.

Nitrogen-group transfer reaction: aziridination

We have previously reported copper-catalyzed aziridination with unstrained complex **4** bearing two independent redox-active iminosemiquinone units and exhibiting a planar geometry around the copper center (Fig. 2b) (Ren *et al.*, 2018). Complex **4** can perform aziridination on a wide range of unactivated alkenes through a mechanism involving molecular spin catalysis, related to the multistate reactivity model encountered in metalloenzymes. Aiming to assess the effect of tetratopic ligand **2** in comparison with two independent ditopic redox-active units, the reactivity of complex **1** in aziridination was therefore investigated.

To examine the influence of ligand strain and redox state, we performed benchmarking reactivity tests under identical conditions on all three possible redox states combinations (SQ/SQ, SQ/BQ and BQ/BQ) of the redox-active units for the unstrained (**4**, **6**, **7**) and strained (**3**, **1**, **5**) complexes (Supplementary Table S10). Strikingly, complex **1** was found to outperform all other complexes, delivering the aziridination adduct **8** of 4-chlorostyrene in quantitative yield. These results suggest that the major reactivity improvement observed with complex **1** is linked to two factors: electronic conjugation between the SQ and BQ redox-active subunits and high steric strain induced by the ligand. Interestingly, the SQ-BQ redox state $Cu(L_{Biphen}SQ\text{-}BQ)^+$ of a functional Galactose oxidase model, was suggested to be involved in the catalytic activity. This model incorporates a biphenyl unit instead of the atropisomeric binaphthyl unit, and thus retains full conjugation between the redox-active subunits but does not exert steric strain as rotation around the arylic C–C bond is possible in the biphenyl unit but not in the atropisomeric binaphtyl unit (Mukherjee, 2008). This provides strong grounds for the role of electronic communication installed between redox-active subunits through the conjugated backbone on the redox state of the reactive complex. The second factor for the major reactivity improvement is the high steric strain observed in complex **1**. This observation is reminiscent of the entatic state model, defined as a strong steric distortion induced by ligands in a metal complex leading to improvement in catalytic activity (Vallee and Williams, 1968).

The scope of the reaction was evaluated (Scheme 1) and revealed the ability of complex **1** to perform aziridination on a wide range of substrates including mono-, di- and trisubstituted double bonds as well as electrophilic functions (**11** and **14**) with yields from 76% up to quantitative (**8**-**10**). Trans-stilbene gave the corresponding *trans* diastereoisomer **12** in 90% yield while *cis*-stilbene provided a mixture of *cis*- and *trans*-aziridines (**12** and **13**), thus pointing towards a probable radical mechanism accounting for *cis*-*trans* isomerization towards the most stable *trans* isomer. Also, conversion of unactivated alkenes (**15** and **17**) could be performed in up to 80% yield, while aziridination of a deactivated substrate afforded the expected product in 38% yield. Tetrasubstituted substrate **18**, unreactive with

complex **4**, was transformed in 86% yield within an hour. Reaction on a geraniol derivative led to products **19** and **20** in higher yield compared to the unstrained complex, and regioselectivity was reinforced towards the less hindered site in accordance with the high steric hindrance in complex **1**. The most striking results are observed when comparing catalysis with strained complex **1** and the most efficient unstrained analogue from our benchmarking reactivity test complex **4** $Cu(SQ)_2$. Reaction time could be divided by up to a factor 8 for compounds **10**, **11**, and **16**-**20**, and yields increased up to a fourty-two-fold (compound **14**), thus demonstrating the efficiency of complex **1**. Based on the substrate scope, average yields of 90% for styrene substrates and 73% for unactivated or hindered substrates are obtained with complex **1** while the unstrained analogue **4** provides much lower average yields (38% and 22% respectively). The calculated average gain in yield observed is 59% and 51% respectively (calculated as the mean value of substracted yields). This indicates that steric strain in complex **1** is accountable for a major reactivity improvement. TON (Turn Over Number) was calculated and found to be significantly and consistently higher in the case of complex **1** versus its unstrained analogue (Scheme 1). The maximum TON value of 20 was found for substrate **8**, along with a TOF (Turn Over Frequency) of 600 h^{-1}. In the case of styrene, we checked that once the aziridination reaction was complete with either complex **1** (after 2 minutes) or complex **4** (after 12 minutes) as a catalyst, addition of new equivalents of styrene and PhINTs led to the formation of the aziridination product in 95% yield for **1** and 82 % yield for **4** : thus, little or no deactivation of the catalyst occurs during the reaction. Since the BINap ligand exhibits axial chirality, the two enantiomers of complex **1** were prepared from commercial enantiopure 1,1'-binaphthyl-2,2'- diamine and the S-isomer was tested in the reaction with 4-chlorostyrene. However, only modest enantiomeric excesses were observed with a maximum 35% ee (Supplementary Table S8). This could be related to the fact that the chirality inducing atropisomeric motif is remote from the coordination sites involved in the reaction, which disfavours enantioselectivity.

Scheme 1. Scope for nitrogen-group transfer with complex 1 and comparison with unstrained analogue 4

Aziridination reaction performed with [a]complex **1** $[CuBINapSQ\text{-}BQ]^+$ (dark blue) ,[b]complex **4** $Cu(SQ)_2$ (pale blue) [c] TON calculated for complexes **1** and **4** [d] ratio of products (numbers in grey). Reaction conditions: 4-chlorostyrene (1 equiv.), PhINTs (2 equiv.), complex (5 mol%), acetonitrile, rt. Yields were determined by ^1H NMR using trimethoxybenzene as internal standard and calculated considering olefin as limiting reactant.

Carbon-group transfer reaction: cyclopropanation

Having established the efficiency of complex **1** in N-group transfer, we investigated its ability to perform C-group transfer with ethyl diazoacetate (EDA), a carbene precursor used in metal-based cyclopropanation reactions. Optimized reaction conditions (Supplementary Tables S11-14) led to the isolation of the cyclopropanated adduct **21** of 4-chlorostyrene in quantitative yield, and the scope of the cyclopropanation reaction was studied (Scheme 2). A wide range of substrates including diverse mono-, and disubstituted styrene derivatives (**21**-**26**), polycyclic (**27**-**28**) substrates as well as unactivated or deactivated tri- and tetrasubstituted scaffolds (**29**-**30**) was efficiently converted. Similarly as before, complex **1** was found to systematically outperform the most efficient unstrained analogue (complex $[Cu(SQ\text{-}BQ)]^+$ in this case) and deliver average yields of 95% and 97% on styrene derivatives and unactivated or hindered substrates respectively, while the unstrained complex reached 67% and 81% average yields respectively. This translated into average gains in yield of 21% and 16% for the two substrate scope categories. The lower gain observed with complex **1** in cyclopropanation compared to aziridination can be explained by the reaction conditions. Reaction yields are assessed over a fixed period of time set by the best performing catalyst and the reaction is stopped upon completion of maximum conversion by the best catalyst (complex **1**). While the aziridination reaction is very fast and can be performed in as fast as 2 min, the cyclopropanation conditions require that the carbene source is added slowly over 20 min to the reaction mixture to avoid unproductive homo-coupling of EDA as side-product. While this accounts for both longer reaction times and decreased gains in yield, complex **1** remains more efficient than the unstrained complex and this is further confirmed by the calculated TON values close to 100 and a calculated TOF of 300 h^{-1} for complex **1** with substrate **21**.

Scheme 2. Scope for carbon-group transfer with complex 1 and comparison with unstrained analogue

Cyclopropanation reaction performed with [a]complex **1** [CuBINapSQ-BQ]$^+$ dark green,[b]complex **6** [Cu(SQ-BQ)]$^+$ pale green, [c]trans/cis ratio. Reaction conditions: 4-chlorostyrene (1 equiv.), EDA (2 equiv.), copper complex (1 mol%), DCM, rt. EDA was added slowly in 20 minutes, reaction time: 20 min. Yields were determined by ^{1}H NMR using trimethoxybenzene as internal standard and calculated considering olefin as limiting reactant.[d]calculated TON for complexes **1** and **6**.

Mechanistic studies

Mechanistically, metal-catalyzed aziridination and cyclopropanation rely on the formation of transient and highly reactive metal-carbene (Dzik *et al.*, 2010; Dzik, Zhang and de Bruin, 2011) and metal-nitrene (Suarez *et al.*, 2013; Goswami *et al.*, 2015; Corona *et al.*, 2016; Kuijpers *et al.*, 2017; Fujita *et al.*, 2018) species, which have been actively investigated in the context of ligand noninnocence. High-resolution mass spectrometry performed on an aliquot of a mixture of complex **1** and excess nitrene (respectively carbene) source at -80°C evidences the presence of a species at m/z 920.3522 (resp. m/z 837.3693) corresponding to the formation of mono-nitrene adduct [**1**-NTs] (respectively mono-carbene adduct [**1**-C(H)CO_2Et]) (Fig. S23, S26). UV-vis studies of complex **1** with the nitrene or carbene sources (Fig. S24, 27-28) show rapid disappearance of the intervalence band around 1200 nm, in agreement with an electron transfer from the BINapSQ-BQ ligand to the nitrene upon coordination thus generating [Cu(BINap-BQ_2)]$^{2+}$ **5**, which does not present any LLCT band. To further assess the efficiency of complex **1**, reaction kinetics were studied by ^{1}H NMR and it was observed that aziridination with complex **1** is complete in less than two minutes (Fig. 3a) while cyclopropanation yields the final product in 20 min upon slow addition of EDA over the course of the reaction (Fig. 3b).

Figure 3. Operando ^{1}H NMR and EPR studies for aziridination (a, c) and cyclopropanation (b, d) of 4-chlorostyrene with complex 1 and kinetic UV-vis studies for aziridination of trans-chalcone with complexes 1 and 4.

The group transfer reactions were studied by continuous wave EPR spectroscopy and operando mode, as our previous work has shown that these techniques can monitor the redox state changes of the complexes and provide structural and kinetic insights into the intermediate species (Fig. 3c and d) (Jacquet, Chaumont, *et al.*, 2016). Regarding the aziridination reaction (Fig. 3c), the first important observation is the absence of spectral differences between the beginning and the end of the reaction (2h), indicating that the catalytic reaction is extremely fast. X-band EPR spectra of complex **1** alone shows that the starting complex is EPR silent from 5 K to room temperature. However, when the aziridination reaction with complex **1** is followed by operando studies (Fig. 3c), two signals are immediately observed: one typical of a Cu^{2+} species (g_{iso} = 2.12 and A_{iso}= 82 G) and the other an organic radical displaying five lines with a coupling of 12.2 G and an intensity ratio of 1 :2 :3 :2: 1. The latter can be attributed to the formation of an organic radical coupled to two magnetically equivalent nitrogens. This suggests that nitrene incorporation instantaneously leads to a Cu^{2+} species with formation a ligand-based radical, these two species not being magnetically coupled. These EPR results indicate fast electron transfer from the starting complex to the nitrene part upon coordination and are consistent with the ^{1}H NMR monitoring of the reaction showing completion of the reaction in 2 min. Operando EPR studies attempted on the cycloproponation reaction were not conclusive as the experimental conditions implying slow addition of EDA could not be reproduced under operando conditions (Fig. 3d). Following the reaction by UV-Vis spectroscopy on trans-chalcone as substrate showed an initial instantaneous reaction rate at least two times higher using complex **1** compared to complex **4** (Fig. 3e and Fig. S20-22). This initial rate enhancement can be directly related to the difference in geometries of the two complexes and points towards a behavior similar to the entatic state, defined as a reactivity improvement arising from strong steric distortion induced by ligands in a metal complex.

Scheme 3. Proposed catalytic cycle for N- and C-group transfer reactions with complex 1. a: Y = -NTs, b: Y = -$CHCO_2Et$.

In light of our combined mechanistic studies, the following general mechanistic scheme can be proposed (Scheme 3). Insertion of the nitrene or carbene group on starting complex **1** generates intermediates **36a-b** (both detected by HRMS), in which the high coordinative strain and torsion angles in complex **1** are released upon reactive group coordination. Intermediates **36a-b** subsequently undergo alkene insertion to yield species **37a-b** (Supplementary Fig. S115 and Table S15), and release the group-transfer product upon ring-closure. DFT calculations (Fig.4) conducted on intermediate **36a** show that one SOMO is perfectly aligned with the Cu-nitrene axis, which reflects the presence of an unpaired electron occupying a metal-based orbital having a Cu $3d_{z^2}$ character. The other SOMO appears mainly distributed over the N-SO_2 group confirming the formation of a nitrene radical moiety (Supplementary Fig. S115-116). This supports the triplet ground spin state of **36a** due to the orthogonal character of the two SOMOs preventing magnetic coupling as observed by EPR spectroscopy. When looking at the electronic structure of **37a**, we observe that the nature of the first SOMO remains metal-centered while the second SOMO is now a delocalized π-orbital distributed over the styrene moiety with the spin density being displaced from the nitrogen to the aryl group upon styrene insertion (Supplementary Fig. S117-118). DFT calculations conducted on intermediate **36b** reveal that one SOMO features a dominant Cu-character and the other one is a ligand-based orbital almost exclusively centered on the carbon atom of the -$CHCO_2Et$ ligand, which supports the formation of a carbene adduct (Supplementary Fig. S119-120). Upon styrene insertion on **36b**, the spin density is shifted towards the carbon center adjacent to the aryl group and the two SOMOs of **37b** appear similar to those of **37a** with one SOMO being metal-centered and the other one being ligand-based delocalized on the styrene moiety (Supplementary Fig. S121-122). Interestingly, a $\Delta\Delta G$ calculation comparing the relative stability of the species obtained upon nitrene and alkene insertion on strained and unstrained complexes **1** and **4** shows that intermediates **36a** and **37a** are stabilized by 2.5 and 7.1 $kcal.mol^{-1}$ respectively, in the case of complex **1** compared to complex **4** (Tables S16-17). These findings highlight the energetic gain observed when using the strained BINap ligand instead of the unstrained SQ, and also reflect that the highly distorted structure induced by coordination of this ligand to the metal center facilitates insertion reactions. Comparison of catalytic efficiency shows that complex **1** compares well with other reported catalytic systems in terms of both reaction time and yield (Table S18).

Figure 4. DFT-calculated spin density plots for intermediates 36a-b and 37a-b.

In conclusion, this report of combines the entatic reactivity model and redox cofactors, which are staples of metalloenzymes' reactivity toolbox, for enhanced group-transfer catalytic transformations. We have demonstrated that an atropisomeric tetratopic redox-active ligand imposing high steric and coordinative strain on a copper center can perform group transfer reactions up to eight times faster than related unstrained systems. The redox-active atropisomeric backbone establishes electronic communication between the two redox-active subunits, thus favoring intramolecular electron transfer during catalysis and maintaining a Cu^{II} redox homeostasis. This system bridges the gap between small-molecule enzymatic structural models focused on the design of the first coordination sphere and top-down approaches achieving control over the aminoacid secondary and tertiary coordination spheres by directed enzymatic evolution (Arnold Frances H., 2017; Farwell *et al.*, 2015; Coelho *et al.*, 2013; Knight *et al.*, 2018). This work shows that the combination of enzymatic reactivity-enabling strategies offers a promising approach to reactivity control in bioinspired catalysis, and should open the door towards more challenging synthetic reactions.

Limitations of the Study

Enantioselective catalysis could not be achieved with this system. Furthermore, the cyclopropanation procedure requires addition of ethyldiazoacetate through syringe pump over a set period of time as to avoid dimerization of the carbene source.

DATA AND SOFTWARE AVAILABILITY

The accession number for the compounds **1** and **2** reported in this paper is CCDC 1906978 and 1906977 (**1**, C2/c and P1 forms) and 1908272 (**2**). These data are provided free of charge by The Cambridge Crystallographic Data Centre.

ACKNOWLEDGMENTS

The authors would like to thank Sorbonne Université (SU), Université de Strasbourg, CNRS, IR-RPE CNRS FR3443 RENARD network (CW X-band EPR with Dr. J.-L. Cantin, INSP UMR CNRS 7588, SU and X-band EPR in Lille). SU is acknowledged for an Emergence grant (M.D.E.M. and K.C.) and CSC for a PhD fellowship (Y.R.). The authors gratefully acknowledge the COST Action 27 CM1305 ECOSTBio and FrenchBIC network. We would also like to thank Dr Vincent Lebrun, CNRS, Université de Strasbourg, for valuable discussions.

AUTHOR CONTRIBUTIONS

Y.R. synthesized and purified the compounds, collected and analysed synthetic and analytical data, performed catalytic experiments and reaction scopes; J.F. performed the X-ray crystallographic analysis; K.C. performed synthetic work, UV-vis studies and analysed the data; N.V. performed the chiral HPLC studies; L.F. analysed the data and commented on the manuscript; H.V. performed the operando EPR studies, analysed the data and wrote the manuscript; M.O. performed the DFT studies, analysed the data and wrote the manuscript; S.B. performed electrochemical and EPR experiments, analysed the data and wrote the manuscript; M.D.E.M. designed the study, analysed the data and wrote the manuscript. All authors contributed to the analysis of the results and commented on the manuscript.

DECLARATION OF INTERESTS

The authors declare no competing interests.

REFERENCES AND NOTES

Adesina, O., Anzai, I. A., Avalos, J. L. and Barstow, B. (2017). Embracing Biological Solutions to the Sustainable Energy Challenge. Chem *2*, 20–51.

Albold, U. *et al.* (2019). Isolable Cu(I) Complexes of Extremely Electron-Poor, Completely Unreduced o-Quinone and "Di-o-Quinone" Ligands Stabilized through π–π Interactions in the Secondary Coordination Sphere. Inorg. Chem. *58*, 3754–3763.

Arnold, F. H. (2017). Directed Evolution: Bringing New Chemistry to Life. Angew. Chem. Int. Ed. *57*, 4143–4148.

Blanchard, S. *et al.* (2012). Non-Innocent Ligands: New Opportunities in Iron Catalysis. *Eur. J. Inorg. Chem.*, 376–389.

Broere, D. L. J., Plessius, R. and van der Vlugt, J. I. (2015). New avenues for ligand-mediated processes – expanding metal reactivity by the use of redox-active catechol, o-aminophenol and o-phenylenediamine ligands. Chem. Soc. Rev. *44*, 6886–6915.

Chaudhuri, P., Hess, M., Flörke, U. and Wieghardt, K. (1998). From Structural Models of Galactose Oxidase to Homogeneous Catalysis: Efficient Aerobic Oxidation of Alcohols. Angew. Chem. Int. Ed. *37*, 2217–2220.

Chaudhuri, P. *et al.* (2001). Electronic Structure of Bis(o-iminobenzosemiquinonato)metal Complexes (Cu, Ni, Pd). The Art of Establishing Physical Oxidation States in Transition-Metal Complexes Containing Radical Ligands. J. Am. Chem. Soc. *123*, 2213–2223.

Chirik, P. J. and Wieghardt, K. (2010). Radical Ligands Confer Nobility on Base-Metal Catalysts. Science *327*, 794–795.

Coelho, P. S., Brustad, E. M., Kannan, A. and Arnold, F. H. (2013). Olefin cyclopropanation via carbene transfer catalysed by engineered cytochrome P450 enzymes. Science *339*, 307–310.

Comba, P. (2000). Coordination compounds in the entatic state. Coord. Chem. Rev. *200–202*, 217–245.

Comba, P. *et al.* (2016). A Bispidine Iron(IV)–Oxo Complex in the Entatic State. Angew. Chem. Int. Ed. *55*, 11129–11133.

Corona, T. *et al.* (2016). Characterization and Reactivity Studies of a Terminal Copper–Nitrene Species. Angew. Chem. Int. Ed. *55*, 14005–14008.

Davidson, V. L. (2018). Protein-Derived Cofactors Revisited: Empowering Amino Acid Residues with New Functions. Biochemistry *57*, 3115–3125.

Dicke, B. *et al.* (2018). Transferring the entatic-state principle to copper photochemistry. Nat. Chem. *10*, 355–362.

Dzik, W. I., Xu, X., Zhang, X. P., Reek, J. N. H. and de Bruin, B. (2010). 'Carbene Radicals' in Co^{II}(por)-Catalyzed Olefin Cyclopropanation. J. Am. Chem. Soc. *132*, 10891–10902.

Dzik, W. I., Zhang, X. P. and de Bruin, B. (2011). Redox Noninnocence of Carbene Ligands: Carbene Radicals in (Catalytic) C−C Bond Formation. Inorg. Chem. *50*, 9896–9903.

Farwell, C. C., Zhang, R. K., McIntosh, J. A., Hyster, T. K. and Arnold, F. H. (2015). Enantioselective enzyme-catalyzed aziridination enabled by active-site evolution of a Cytochrome P450. ACS Cent. Sci. *1*, 89-93.

Freiberger, M. I., Guzovsky, A. B., Wolynes, P. G., Parra, R. G. and Ferreiro, D. U. (2019). Local frustration around enzyme active sites. Proc. Natl. Acad. Sci. *116*, 4037–4043.

Fujita, D., Sugimoto, H., Morimoto, Y. and Itoh, S. (2018). Noninnocent Ligand in Rhodium(III)-Complex-Catalyzed C–H Bond Amination with Tosyl Azide. Inorg. Chem. *57*, 9738–9747.

Garcia, L. *et al.* (2015). Entasis through Hook-and-Loop Fastening in a Glycoligand with Cumulative Weak Forces Stabilizing Cu^{I}. J. Am. Chem. Soc. *137*, 1141–1146.

Goswami, M. *et al.* (2015). Characterization of Porphyrin-Co(III)-'Nitrene Radical' Species Relevant in Catalytic Nitrene Transfer Reactions. J. Am. Chem. Soc. *137*, 5468–5479.

Grützmacher, H. (2008). Cooperating Ligands in Catalysis. Angew. Chem. Int. Ed. *47*, 1814–1818.

Hoffmann A. *et al.* (2013) Catching an Entatic State—A Pair of Copper Complexes. Angew. Chem. Int. Ed. *53*, 299–304.

Jacquet, J., Blanchard, S., Derat, E., Desage-El Murr, M. and Fensterbank, L. (2016). Redox-ligand sustains controlled generation of CF_3 radicals by well-defined copper complex. Chem. Sci. *7*, 2030–2036.

Jacquet, J. *et al.* (2016). C−N Bond Formation from a Masked High-Valent Copper Complex Stabilized by Redox Non-Innocent Ligands. Angew. Chem. Int. Ed. *55*, 10712–10716.

Jacquet, J. *et al.* (2017). Circumventing Intrinsic Metal Reactivity: Radical Generation with Redox-Active Ligands. Chem. – Eur. J. *23*, 15030–15034.

Kaim, W. (2011). Manifestations of Noninnocent Ligand Behavior. Inorg. Chem. *50*, 9752–9765.

Knight, A. M., Kan, S. B. J., Lewis, R. D., Brandenberg, O. F., Chen, K. and Arnold, F. H. (2018). Diverse engineered heme proteins enable stereodivergent cyclopropanation of unactivated alkenes. ACS Cent. Sci. *4*, 372-377.

Kuijpers, P., van der Vlugt, J. I., Schneider, S. and de Bruin, B. (2017). Nitrene Radical Intermediates in Catalytic Synthesis. Chem. – Eur. J. *23*, 13819–13829.

Luca, O. R. and Crabtree, R. H. (2012). Redox-active ligands in catalysis. Chem. Soc. Rev. *42*, 1440–1459.

Lyaskovskyy, V. and de Bruin, B. (2012). Redox Non-Innocent Ligands: Versatile New Tools to Control Catalytic Reactions. ACS Catal. *2*, 270–279.

Malachowski, M.R., Adams, M., Elia, N., Rheingold A.L. and Kelly, R.S. (1999). Enforcing geometrical constraints on metal complexes using biphenyl-based ligands: spontaneous reduction of copper(II) by sulfur-containing ligands. *J. Chem. Soc. Dalton Trans.*, 2177–2182.

Mara, M. W. *et al.* (2017). Metalloprotein entatic control of ligand-metal bonds quantified by ultrafast x-ray spectroscopy. Science *356*, 1276–1280.

Mukherjee, C., Weyhermüller, T., Bothe, E. and Chaudhuri, P. (2008). Targeted Oxidase Reactivity with a New Redox-Active Ligand Incorporating N2O2 Donor Atoms. Complexes of Cu(II), Ni(II), Pd(II), Fe(III), and V(V). Inorg. Chem. *47*, 11620–11632.

Müller, E., Bernardinelli, G. and Reedijk, J. (1996). 2,2'-Bis(3-(2-pyridyl)-1-methyltriazolyl)biphenyl: A Tetracoordinating Wrapping Ligand Inducing Similar Skew Coordination Geometries at Copper(I) and Copper(II). *Inorg. Chem. 35*, 1952–1957.

Müller, E., Piguet, C., Bernardinelli, G. and Williams, A.F. (1988). 2,2'-Bis(6-(2,2'-bipyridyl))biphenyl (TET), a sterically constricted tetradentate ligand: structures and properties of its complexes with copper(I) and copper(II). *Inorg. Chem. 27*, 849–855.

Praneeth, V. K. K., Ringenberg, M. R. and Ward, T. R. (2012). Redox-Active Ligands in Catalysis. Angew. Chem. Int. Ed. *51*, 10228–10234.

Ren, Y. *et al.* (2018). Copper-Catalyzed Aziridination with Redox-Active Ligands: Molecular Spin Catalysis. Chem. – Eur. J. *24*, 5086–5090.

Rudroff, F. *et al.* (2018). Opportunities and challenges for combining chemo- and biocatalysis. Nat. Catal. *1*, 12–22.

Schrempp David F. *et al.* (2017). Inter- and Intramolecular Electron Transfer in Copper Complexes: Electronic Entatic State with Redox-Active Guanidine Ligands. Chem. – Eur. J. *23*, 13607–13611.

Snyder, B. E. R. *et al.* (2016). The active site of low-temperature methane hydroxylation in iron-containing zeolites. Nature *536*, 317–321.

Stanek, J., Hoffmann, A. and Herres-Pawlis, S. (2018). Renaissance of the entatic state principle. Coord. Chem. Rev. *365*, 103–121.

Stanek J. *et al.* (2017). Copper Guanidinoquinoline Complexes as Entatic State Models of Electron-Transfer Proteins. Chem. – Eur. J. *23*, 15738–15745.

Stubbe, J. and van der Donk, W. A. (1998). Protein Radicals in Enzyme Catalysis. Chem. Rev. *98*, 705–762.

Suarez, A. I. O., Lyaskovskyy, V., Reek, J. N. H., van der Vlugt, J. I. and de Bruin, B. (2013). Complexes with Nitrogen-Centered Radical Ligands: Classification, Spectroscopic Features, Reactivity, and Catalytic Applications. Angew. Chem. Int. Ed. *52*, 12510–12529.

Vallee, B. L. and Williams, R. J. (1968). Metalloenzymes: the entatic nature of their active sites. Proc. Natl. Acad. Sci. *59*, 498–505.

van der Vlugt, J. I. (2012). Cooperative Catalysis with First-Row Late Transition Metals. Eur. J. Inorg. Chem., 363–375.

van der Vlugt, J. I. (2019) 'Radical-Type Reactivity and Catalysis by Single-Electron Transfer to or from Redox-Active Ligands', Chemistry – A European Journal, *25*, 2651–2662.

Wang, Y., DuBois, J. L., Hedman, B., Hodgson, K. O. and Stack, T. D. P. (1998). Catalytic Galactose Oxidase Models: Biomimetic Cu(II)-Phenoxyl-Radical Reactivity. Science *279*, 537–540.

Williams, R. J. P. (1971). Catalysis by metallo-enzymes: The entatic state. Inorganica Chim. Acta Rev. *5*, 137–155.

Williams, R. J. P. (1995). Energised (entatic) States of Groups and of Secondary Structures in Proteins and Metalloproteins. Eur. J. Biochem. *234*, 363–381.

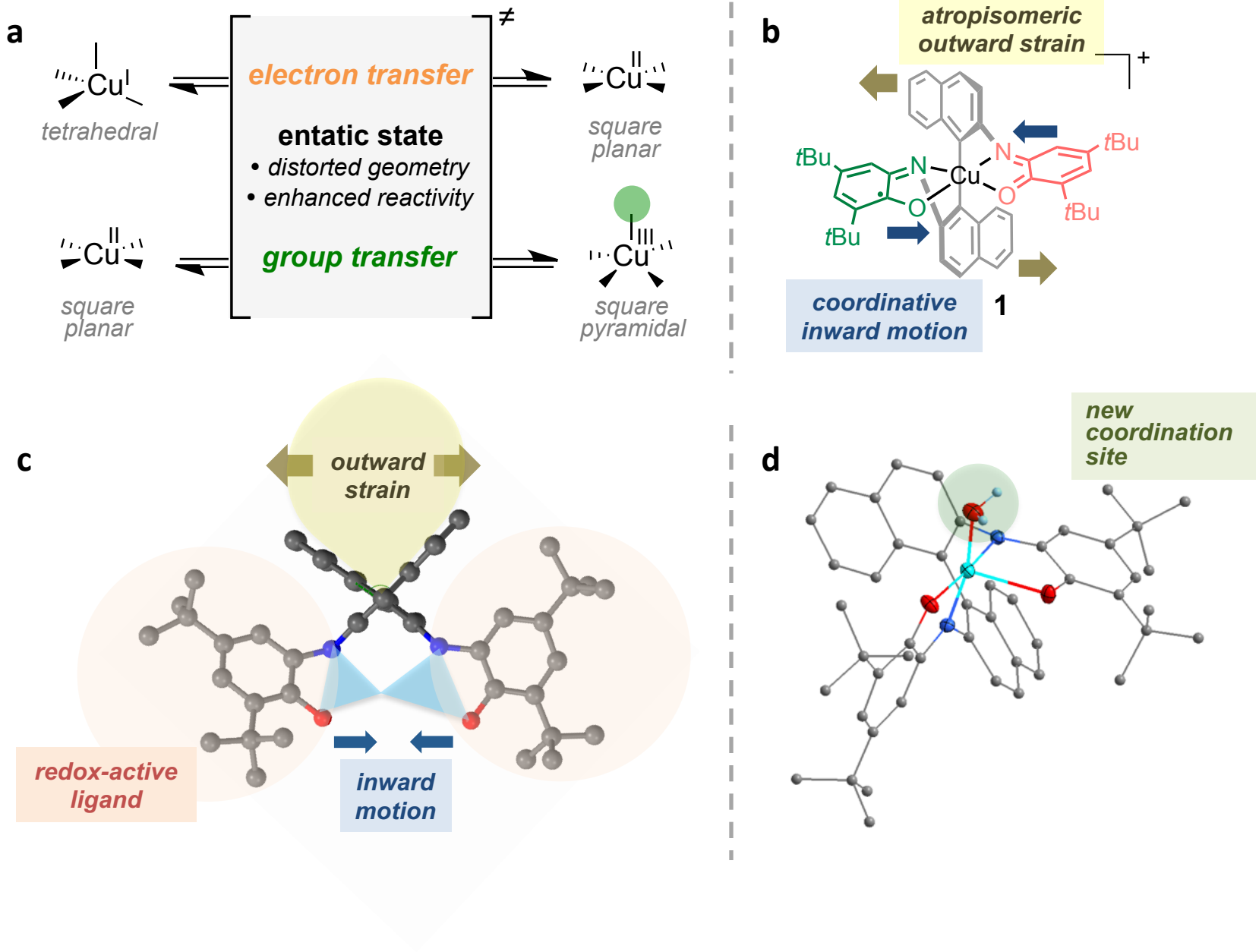
a
Cu
tetrahedral
electron transfer
entatic state
• distorted geometry
• enhanced reactivity
group transfer
square planar
square planar
square pyramidal
b
atropisomeric outward strain
+
tBu
tBu
tBu
tBu
N
N
Cu
O
O
coordinative inward motion
1
c
outward strain
redox-active ligand
inward motion
d
new coordination site

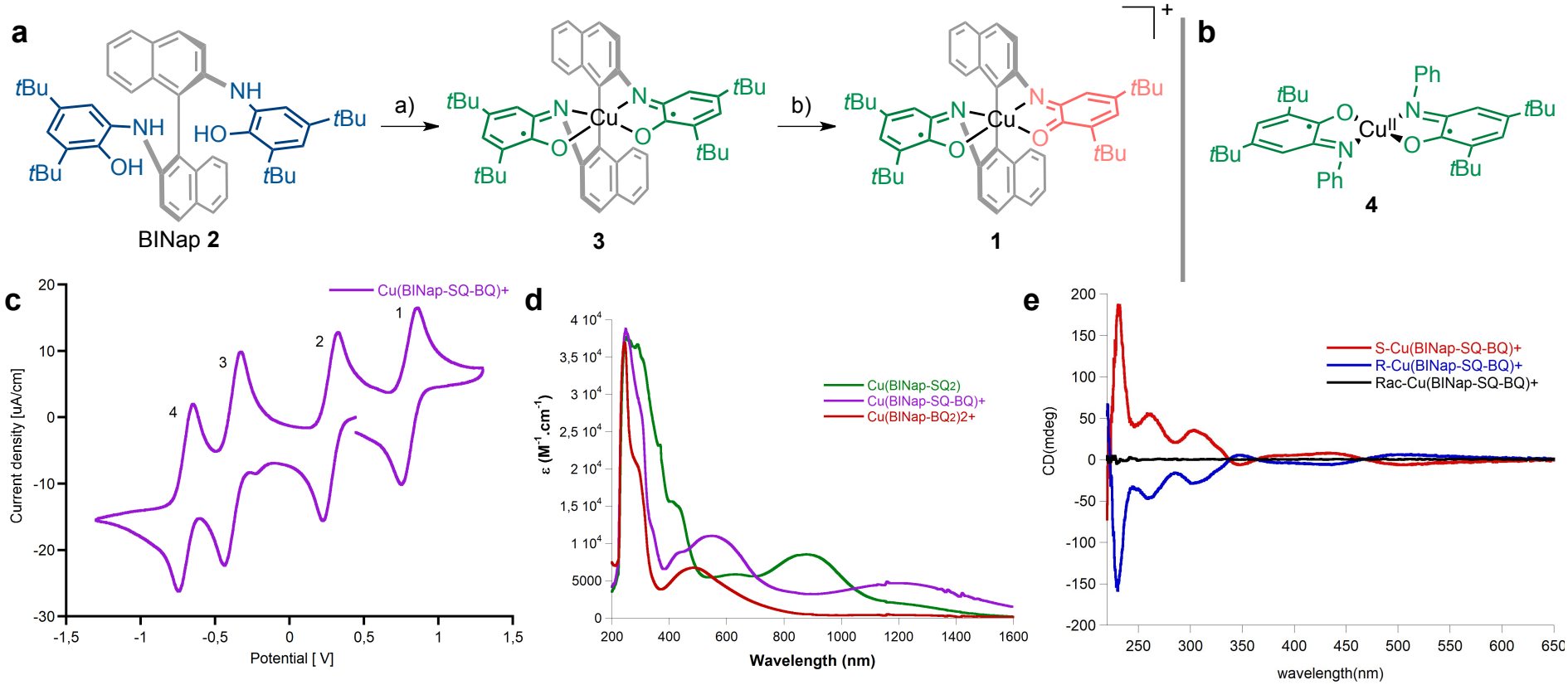
a
tBu
NH
NH
HO
tBu
tBu
OH
tBu
BINap 2
a)
tBu
N
Cu
N
tBu
O
O
tBu
tBu
3
b)
tBu
N
Cu
N
tBu
O
O
tBu
+
1
b
tBu
O
Cu
II
Ph
N
tBu
N
O
tBu
Ph
4
c
Cu(BINap-SQ-BQ)+
1
2
3
4
Current density [uA/cm]
Potential [V]
d
Cu(BINap-SQ2)
Cu(BINap-SQ-BQ)+
Cu(BINap-BQ2)2+
ε (M-1.cm-1)
Wavelength (nm)
e
S-Cu(BINap-SQ-BQ)+
R-Cu(BINap-SQ-BQ)+
Rac-Cu(BINap-SQ-BQ)+
CD(mdeg)
wavelength(nm)

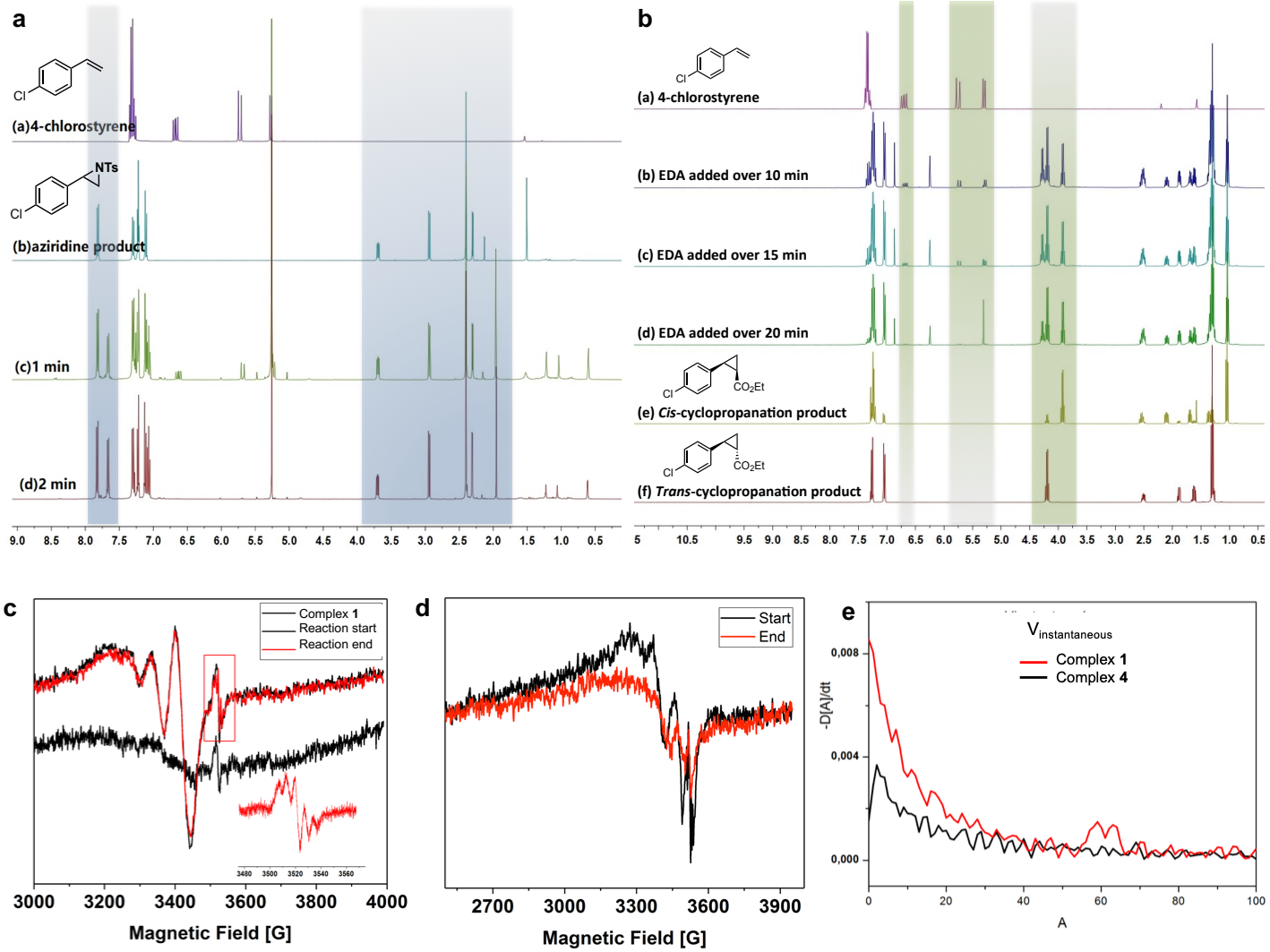
a
(a)4-chlorostyrene
(b)aziridine product
(c)1 min
(d)2 min
b
(a) 4-chlorostyrene
(b) EDA added over 10 min
(c) EDA added over 15 min
(d) EDA added over 20 min
(e) Cis-cyclopropanation product
(f) Trans-cyclopropanation product
c
Complex 1
Reaction start
Reaction end
Magnetic Field [G]
d
Start
End
Magnetic Field [G]
e
V instantaneous
Complex 1
Complex 4
-D[A]/dt
A

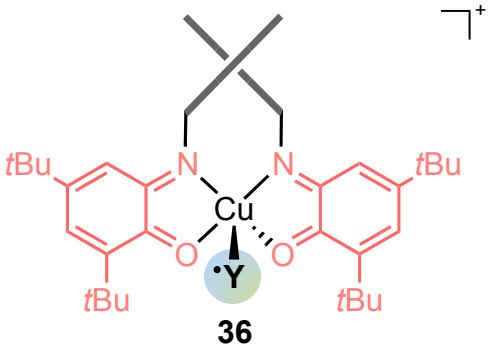

36

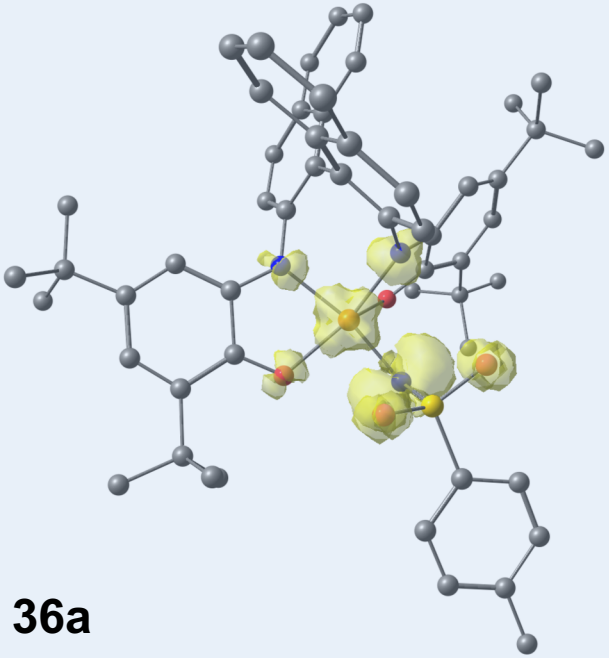

36a

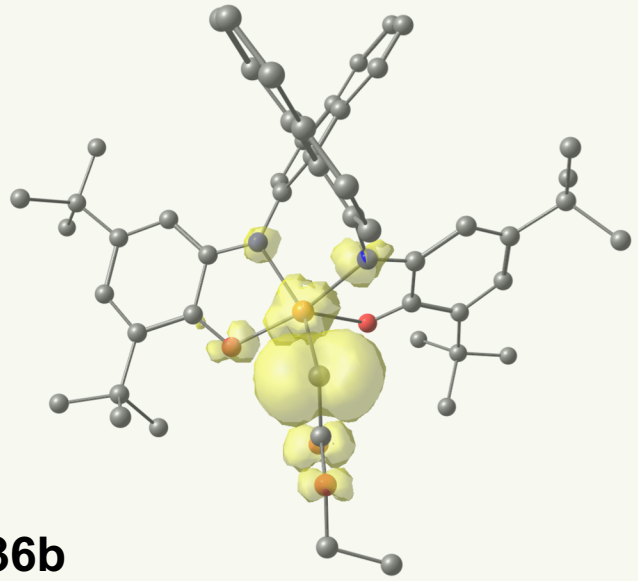

36b

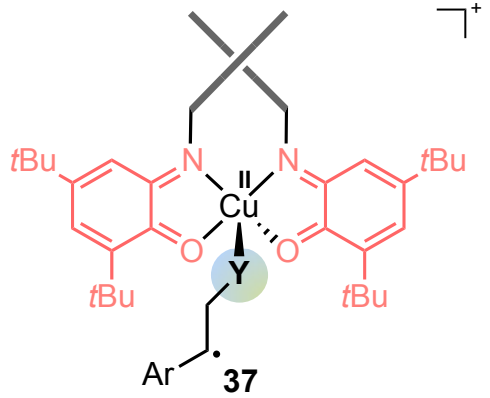

37

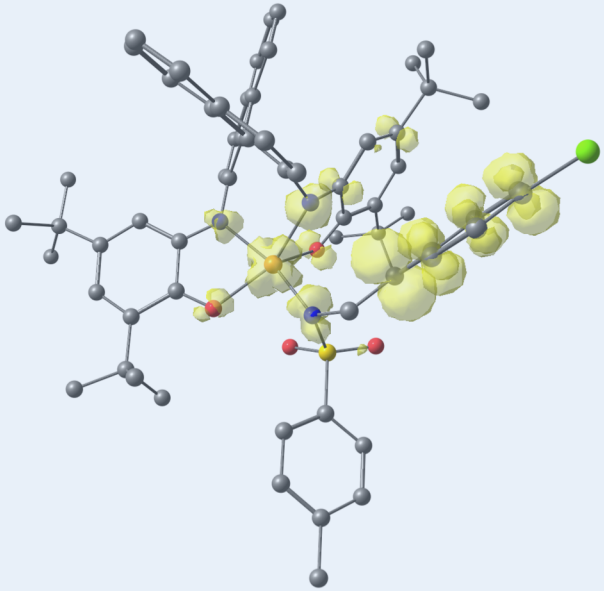

37a **Y** = -NTs

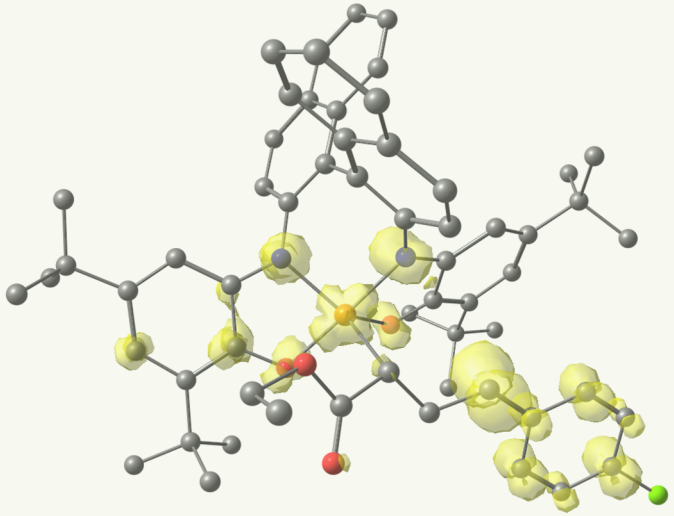

37b **Y** = -$CHCO_2Et$

Styrene substrates

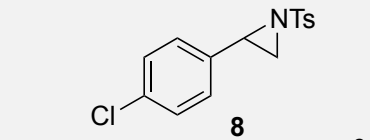

8

2 min — >99%[a]
44%[b]
TON[c] 20 / 9

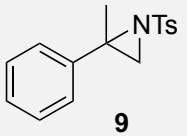

9

2 h — 96%
31%
19 / 6

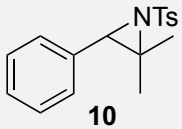

10

8 h — 76%
15 h — 29%
15 / 6

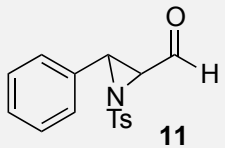

11

7 h — 71%
31%
14 / 6

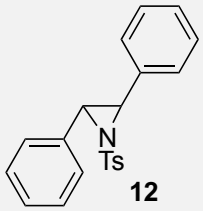

12

1 h — 90%
74%
from *trans*-stilbene
18 / 15

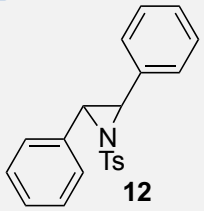

12

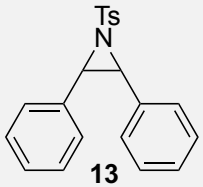

13

1 h — 99% 58:42[d]
59% 54:46
from *cis*-stilbene
20 / 12

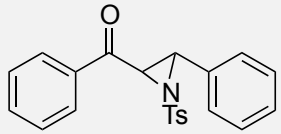

14

1 h — 85%
2%
from *trans* -1,3-diphenyl-2-propen-1-ol
17 / 1

1 h — 99%
34%
from *trans*-chalcone
20 / 7

Average yields

90% strained

38% unstrained

59% average gain in yield

Unactivated / deactivated / sterically hindered substrates

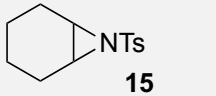

15

3 h — 75%
22%
15 / 4

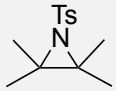

18

1 h — 86%
0%
17 / 0

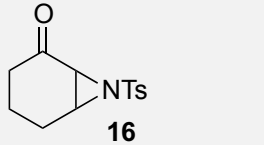

16

8 h — 38%
15 h — 12%
8 / 2

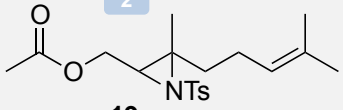

19

6 h — 86% 14:86[c]
27% 18:82
17 / 5

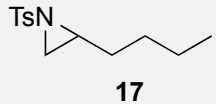

17

2 h — 80%
48%
16 / 10

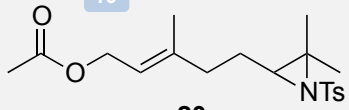

20

73% strained

22% unstrained

51% average gain in yield

Styrene and aromatic substrates

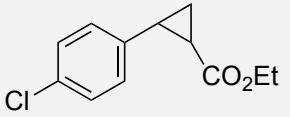

21

>99%[a] (59:41)[c]
75%[b] (64:36)
100[d]
75

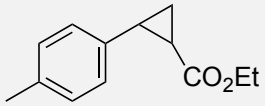

22

>99% (58:42)
71% (62:38)
100
71

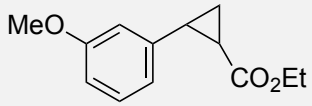

23

>99% (60:40)
65% (63:37)
100
65

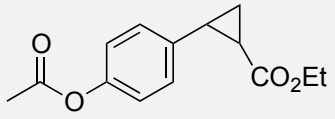

24

91% (59:41)
65% (60:40)
91
65

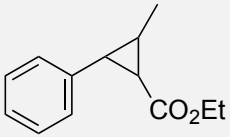

25

83% 63:37
49% 66:34
83
49

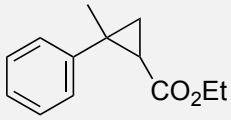

26

>99% 53:47
73% 53:47
100
73

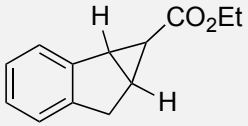

27

>99% 72:28
75% 72:28
100
75

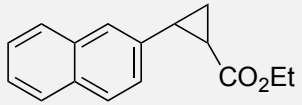

28

91% 60:40
63% 61:39
91
63

Average yields

95%
strained

67%
unstrained

21%
average gain in yield

Unactivated / deactivated / sterically hindered substrates

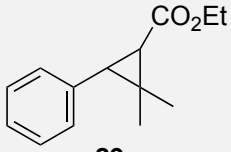

29

75% 58:42
41% 60:40
75
41

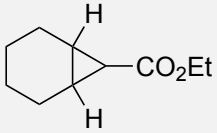

30

>99% 96:4
85% 96:4
100
85

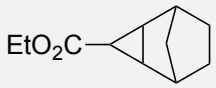

31

>99% 53:47
87% 60:40
100
87

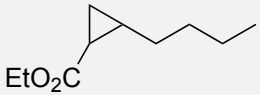

32

>99% 56:44
91% 59:41
100
91

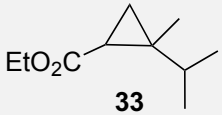

33

>99% 50:50
92% 50:50
100
92

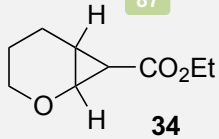

34

>99% 91:9
90% 91:9
100
90

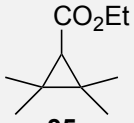

35

>99%
84%
100
84

97%
strained

81%
unstrained

16%
average gain in yield

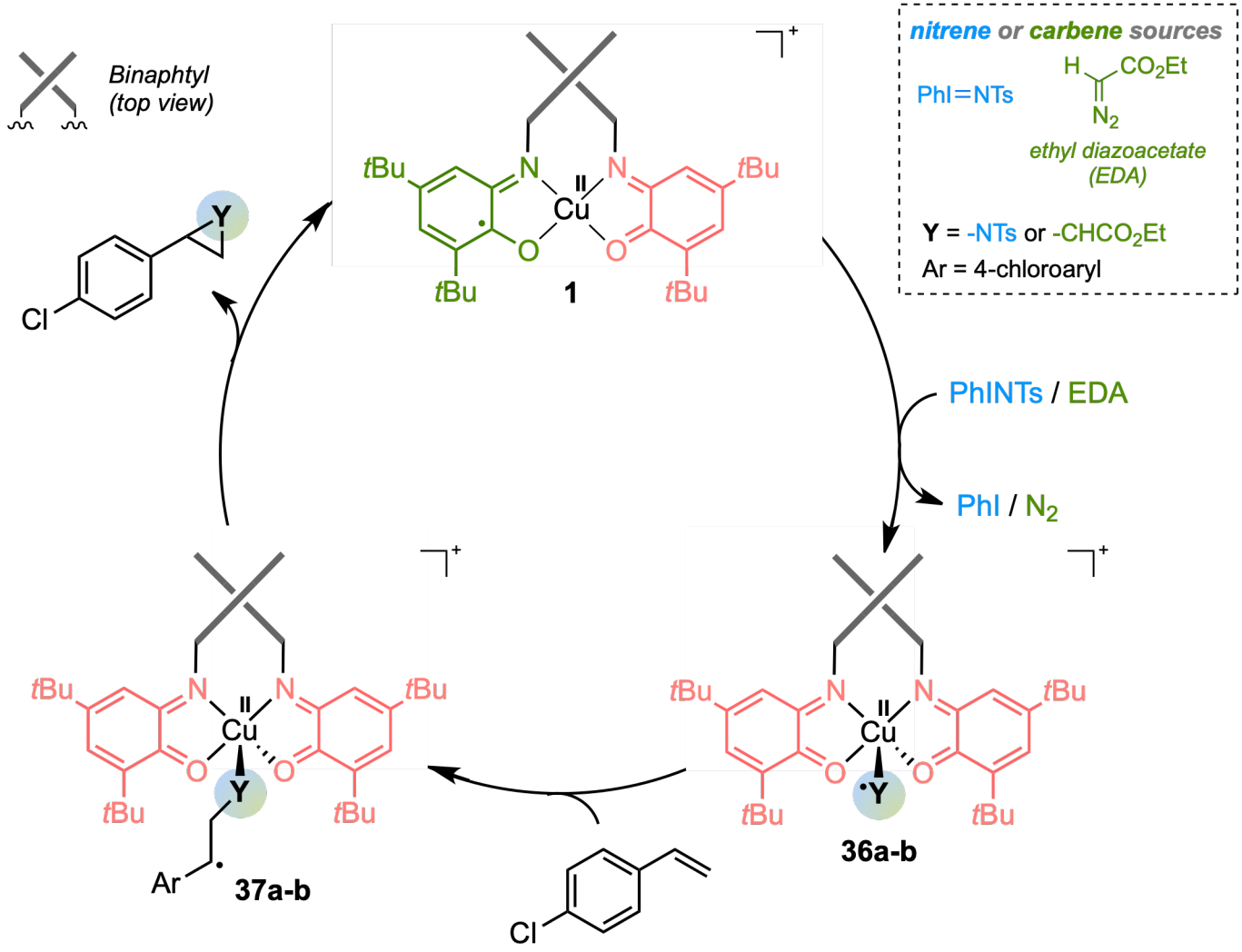
Binaphtyl
(top view)
nitrene or carbene sources
PhI=NTs
H
CO2Et
N2
ethyl diazoacetate
(EDA)
Y = -NTs or -CHCO2Et
Ar = 4-chloroaryl
tBu
N
Cu
O
1
PhINTs / EDA
PhI / N2
Cl
Y
36a-b
37a-b
Ar

HIGHLIGHTS

- We design a catalyst interfacing two reactivity-enhancing tools from metalloenzymes
- This work merges redox-active cofactors and entatic state reactivity
- The modifications in the coordination sphere lead to enhanced catalytic behavior
- These results open perspectives in bioinspired catalysis and group-transfer reactions